Molecular Imaging and Biology
https://doi.org/10.1007/s11307-024-01932-y

RESEARCH ARTICLE

A Feasibility Study of [^{18}F]F-AraG Positron Emission Tomography (PET) for Cardiac Imaging–Myocardial Viability in Ischemia–Reperfusion Injury Model

Uttam M. Shrestha[1] · Hee-Don Chae[2] · Qizhi Fang[3] · Randall J. Lee[3] · Juliet Packiasamy[2] · Lyna Huynh[2] · Joseph Blecha[1] · Tony L. Huynh[1] · Henry F. VanBrocklin[1] · Jelena Levi[2] · Youngho Seo[1]

Received: 11 April 2024 / Revised: 5 June 2024 / Accepted: 1 July 2024

Abstract

Purpose Myocardial infarction (MI) with subsequent inflammation is one of the most common heart conditions leading to progressive tissue damage. A reliable imaging marker to assess tissue viability after MI would help determine the risks and benefits of any intervention. In this study, we investigate whether a new mitochondria-targeted imaging agent, ^{18}F-labeled 2'-deoxy-2'-^{18}F-fluoro-9-β-d-arabinofuranosylguanine ([^{18}F]F-AraG), a positron emission tomography (PET) agent developed for imaging activated T cells, is suitable for cardiac imaging and to test the myocardial viability after MI.

Procedure To test whether the myocardial [^{18}F]-F-AraG signal is coming from cardiomyocytes or immune infiltrates, we compared cardiac signal in wild-type (WT) mice with that of T cell deficient *Rag1* knockout (*Rag1* KO) mice. We assessed the effect of dietary nucleotides on myocardial [^{18}F]F-AraG uptake in normal heart by comparing [^{18}F]F-AraG signals between mice fed with purified diet and those fed with purified diet supplemented with nucleotides. The myocardial viability was investigated in rodent model by imaging rat with [^{18}F]F-AraG and 2-deoxy-2[^{18}F]fluoro-D-glucose ([^{18}F]FDG) before and after MI. All PET signals were quantified in terms of the percent injected dose per cc (%ID/cc). We also explored [^{18}F]FDG signal variability and potential T cell infiltration into fibrotic area in the affected myocardium with H&E analysis.

Results The difference in %ID/cc for *Rag1* KO and WT mice was not significant (p = ns) indicating that the [^{18}F]F-AraG signal in the myocardium was primarily coming from cardiomyocytes. No difference in myocardial uptake was observed between [^{18}F]F-AraG signals in mice fed with purified diet and with purified diet supplemented with nucleotides (p = ns). The [^{18}F]FDG signals showed wider variability at different time points. Noticeable [^{18}F]F-AraG signals were observed in the affected MI regions. There were T cells in the fibrotic area in the H&E analysis, but they did not constitute the predominant infiltrates.

Conclusions Our preliminary preclinical data show that [^{18}F]F-AraG accumulates in cardiomyocytes indicating that it may be suitable for cardiac imaging and to evaluate the myocardial viability after MI.

Keywords [^{18}F]FDG · [^{18}F]F-AraG · Myocardial infarction · Inflammation · Cardiac metabolism · T cell infiltration

Introduction

Left ventricular (LV) dysfunction associated with ischemia holds a major clinical significance as this is one of the most common causes of myocardial infarction (MI) and sudden death [1]. Patients after MI are at substantially elevated risks of developing ischemic cardiomyopathy, long-term complications, and comorbidities [2]. Restoration of myocardial perfusion and functional recovery in the aggravated cardiomyocytes is feasible through percutaneous coronary intervention (PCI) such as angioplasty, coronary artery bypass graft (CABG) or other means of therapy. The success rate of

✉ Uttam M. Shrestha
ums37uconn@gmail.com

✉ Jelena Levi
jlevi@cellsighttech.com

[1] Department of Radiology and Biomedical Imaging, UCSF Physics Research Laboratory, University of California, 185 Berry Street, STE 350, San Francisco, CA 94143, USA

[2] CellSight Technologies, Inc., 185 Berry Street, STE 350, San Francisco, CA 94107, USA

[3] Department of Medicine, Cardiovascular Research Institute, University of California, San Francisco, CA, USA

Published online: 26 July 2024

these procedures, however, remains controversial due to lack of precise knowledge of tissue viability [3]. Besides, a significant risk is associated with such procedure especially in comorbid patients with multivessel coronary artery disease (CAD) [4]. Nevertheless, there is a notable improvement in patients with documented evidence of myocardial viability after revascularization [5]. It is therefore beneficial to develop a noninvasive imaging marker to determine whether the dysfunctional myocardium is non-viable in which case the risks of intervention would likely be greater than the benefits.

Delineation of a clear boundary between viable myocardium and fibrotic scar in the post-MI patients is clinically challenging [6, 7]. A number of imaging methods have been utilized that enable the localization and semi-quantification of the viability of myocardium [8–11]. The commonly used modalities for assessing myocardial viability are cardiac magnetic resonance (CMR), dobutamine stress echocardiography (ECG), single photon emission computed tomography (SPECT) with ^{99m}Tc-Sestamibi, and positron emission tomography (PET) with 2-deoxy-2[^{18}F]fluoro-D-glucose ([^{18}F]FDG) [12]. [^{18}F]FDG PET is routinely used clinically to assess myocardial viability after MI, as it detects tissue with preserved glucose metabolism. However, [^{18}F]FDG uptake is affected by blood glucose levels which necessitates careful management of glucose levels before the scan. This task can be particularly challenging in patients with diabetes, a population at higher risk for cardiovascular diseases, including MI.

Since myocardium has immense mitochondrial activity, we hypothesized that mitochondria-targeted PET imaging agent, ^{18}F-labeled 2'-deoxy-2'-^{18}F-fluoro-9-β-d-arabinofuranosylguanine ([^{18}F]F-AraG), may be useful in cardiac imaging and assessment of myocardial viability. [^{18}F]F-AraG molecules enter cells via nucleoside transporters and get phosphorylated by mitochondrial deoxyguanosine kinase (dGK) (Fig. 1). Triphosphorylated [^{18}F]F-AraG can be incorporated into mtDNA enabling the assessment of mitochondrial biogenesis [13, 14]. [^{18}F]F-AraG was originally developed for imaging activated T cells [15, 16], and has been evaluated in a number of preclinical models including response to immune checkpoint inhibitor therapy [17], acute graft-versus-host disease [14], immunomodulation and tumor profiling [18], arthritis [19] and multiple sclerosis [20]. [^{18}F]F-AraG was also investigated in healthy human subjects [13, 21], cancer patients [22] and in COVID–19 convalescent subjects [23].

Here we show, in a preclinical model, that [^{18}F]F-AraG accumulates in cardiomyocytes and that it may be suitable to test the myocardial viability after MI. We also explore inflammatory cell infiltration into myocardium post tissue injury, focusing on T cells and assess the effects of dietary nucleotides on [^{18}F]F-AraG myocardial signal.

Materials and Methods

All animal procedures were approved by the UCSF Institutional Animal Care and Use Committee (IACUC), and animal housing and care were provided by UCSF Laboratory Animal Resource Center (LARC). All animals were housed in a specific pathogen-free environment and used at the age between 6 to 9 weeks for mice and 4 to 6 months for rats.

[^{18}]F-Arag was synthesized at the UCSF Radiopharmaceutical Facility in accordance with the Food and Drug Administration (FDA) approved Investigational New Drug (IND)'s chemistry manufacturing and control (CMC) processes [13, 24].

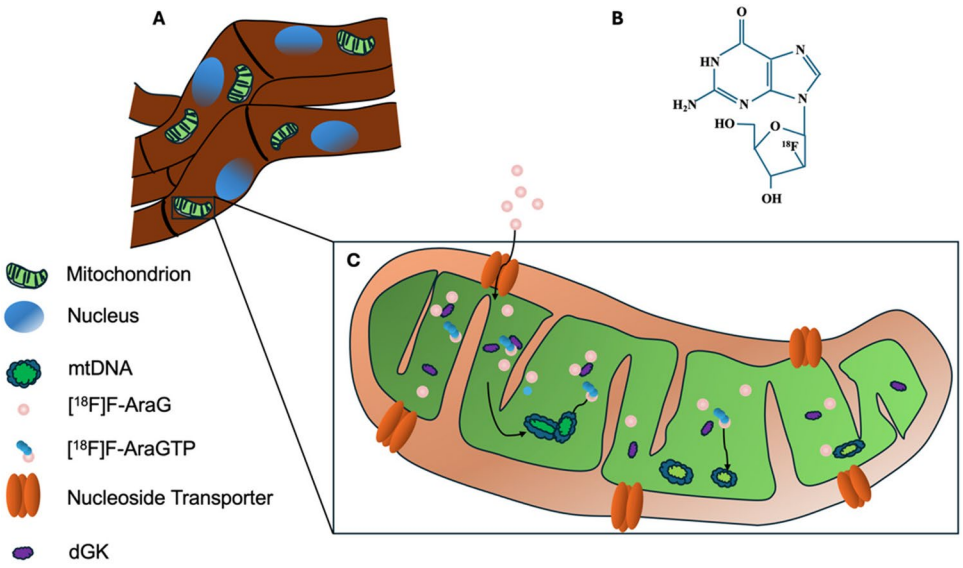

Fig. 1 Mechanism of [^{18}F]F-AraG uptake in cardiomyocytes (**A**) and [^{18}F]F-AraG molecular structure (**B**). [^{18}F]F-AraG molecules enter cells through nucleoside transporters and are subsequently modified by mitochondrial deoxyguanosine kinase (dGK), leading to the formation of [^{18}F]F-AraGTP within the mitochondria that can get incorporated into mtDNA during the process of biogenesis (**C**)

[^{18}F]F-AraG Myocardial Signal in Wildtype (WT) vs. *Rag1* knockout (*Rag1* KO) Mice

To test whether the myocardial [^{18}F]F-AraG uptake in normal heart is coming from cardiomyocytes or from T cells, 8 *C57BL/6 J* wild-type (WT) mice (6 to 8 weeks old, 4 M, 4F) and 4 *C57BL/6 J recombination activating gene 1* knockout (*Rag1* KO) mice (6 to 8 weeks old, 4 F) were purchased from Jackson Laboratory (Bar Harbor, ME).

Effects of Dietary Nucleotides on [^{18}F]F-AraG Myocardial Signal

We assessed the impact of dietary nucleotides on [^{18}F]F-AraG myocardial signal. For this purpose, we obtained 10 *C57BL/6 J* female mice (6 to 9 weeks old) from Jackson Laboratory (Bar Harbor, ME), and randomly allocated them into two experimental groups. The mice in the first group were fed a purified diet (AIN-94G purified diet; Envigo, Indianapolis, IN) supplemented with 0.04% (weight/weight) nucleotides (PD + NT) for 4 days, while the mice in the second group were fed a purified diet without nucleotide (PD).

Rodent Model for Myocardial Infarction

To test whether [^{18}F]F-AraG accumulates in viable cardiomyocytes, 6 healthy Sprague–Dawley male rats (4 to 6 months old) were purchased from Charles River Laboratories (Wilmington, MA) and underwent occlusion-reperfusion surgery. Following anaesthetization and intubation, a left-sided thoracotomy was performed to each rat, and the left coronary artery (LCA) was ligated for 120 min and reopened to ensure an ischemia–reperfusion induced MI [25]. The LCA ligation prevents mid-distal perfusion causing hypoxia in a moderate to large portion of the distal LV regions resulting in reversible (or irreversible) cardiomyocyte damage. After surgery, the animals were transferred back to animal housing and allowed to recover for about a week until further PET scans were performed.

[^{18}F] F-AraG and [^{18}F] FDG Myocardial PET Imaging

All *in vivo* [^{18}F]F-AraG and [^{18}F]FDG imaging were performed at different imaging sessions using microPET/CT scanners (Inveon, Siemens Medical Solutions or nanoScan, Mediso USA) with established standard operating procedures. All animals were fed the same diet and were anesthetized using the same procedures (isoflurane). For [^{18}F]FDG imaging, overnight fasting was implemented but glucose levels were not controlled or measured before image acquisition. A similar protocol was implemented for [^{18}F]F-AraG but without overnight fasting.

For animal procedure, an angiocatheter was placed into the caudal vein to ensure intravenous administration of radiopharmaceuticals. The catheter placement was checked by flushing a small amount of saline solution.

An approximate dose of 45 MBq/rat [^{18}F]F-AraG and 7.5 MBq/mouse of [^{18}F]F-AraG were administered intravenously. One hour after [^{18}F]F-AraG injection, static PET/CT scans focusing on the heart (15 min PET acquisition and 10 min CT scan for anatomic reference) were acquired. The same imaging protocol was implemented for [^{18}F]FDG imaging with an approximate dose of 30 MBq/rat. Rats were fasted overnight prior to [^{18}F]FDG PET scans to reduce plasma glucose levels. All six rats underwent both [^{18}F]F-AraG and [^{18}F]FDG imaging before surgery for the baseline study. However, only 4 rats were imaged after surgery because of mortality of 2 rats.

PET data were reconstructed using a standard reconstruction algorithm and post-processed with methods provided by the manufacturer. CT-based attenuation correction was also implemented to minimize attenuation artifacts. For image analysis and quantification, data were imported into open source software such as Amide [26]. Whenever quantification is mandated, PET signals were expressed as the percent injected activity per cc (%ID/cc). Volumes of interest (VOIs) were set using the thresholding methods in a semiquantitative fashion. MI volumes were defined with activity below 50% of the peak activity value. For regional assessment, hearts were segmented, and data were analyzed using the 17-segment model of heart (AHA) with the PMOD cardiac PET tool (PCARDP, PMOD technologies, Zurich, Switzerland).

Immunohistochemistry

Immunohistochemistry and hematoxylin–eosin (H&E) staining were performed by VitroVivo Biotech (Rockville, MD). Frozen sections were fixed with cold acetone/methanol mixture (1:1) for 15 min. Antigen retrieval was performed by heat inactivation in citrate buffer (10 mM citrate buffer (pH 6.0), 0.05% Tween 20; boiled in microwave with high power for 3 min and maintain at 95 °C in steamer for 15 min). Following blocking with goat serum, the sections were incubated with rabbit anti-CD3 antibody (#ab16669, 1:800, Abcam, Boston, MA) at 4 °C overnight. Then, endogenous peroxidase was blocked with hydrogen peroxide (1% in PBS for 15 min). The sections were then incubated with goat anti-rabbit IgG ImmPRESS™ Secondary Antibody for 1 h at room temperature

and subsequently stained using 3,3' diaminobenzidine and counterstained with Mayer's hematoxylin solution. Images were captured with a 40× objective on an Olympus VS120 microscope scanner using VS-ASW (Olympus, Japan).

Statistical Analysis

Any uptake sample quantification was expressed as mean ± SD. Whenever necessary, *p*-values were calculated using two-tailed t-test and Wilcoxon rank-sum test for comparing two independent groups of samples to draw the statistical significance. Any difference was considered statistically significant if the *p*-value was less than 0.05. Any *p*-value less than 0.001 was expressed as $p < 0.001$. All statistical calculations were performed using the Microsoft Excel and open-source statistical package R.

Results

[^{18}F]F-AraG Myocardial Signal in WT vs. *Rag1* KO Mice

As [^{18}F]F-AraG was originally developed as a tracer for activated T cells, we first investigated whether the [^{18}F]F-AraG signal in the myocardium is coming from cardiomyocytes or T cells. To do so, we compared myocardial [^{18}F]F-AraG uptake in wildtype (WT) mice ($n=8$; 4F, 4 M) with the cardiac uptake in T cell-deficient, *Rag1* KO mice ($n=4$; 4F). The %ID/cc for *Rag1* KO was slightly lower compared to WT mice, but the difference was not statistically significant (4.38 ± 0.84 vs. 4.93 ± 0.73, $p=0.29$) indicating that the [^{18}F]F-AraG signal in the myocardium was primarily coming from cardiomyocytes (Fig. 2).

Comparison of [^{18}F]F-AraG and [^{18}F]FDG Signal Variability

To better understand utility of [^{18}F]F-AraG in cardiac imaging we compared the [^{18}F]F-AraG and [^{18}F]FDG signals in the myocardium of rat before and after MI. The overall timeline for the rat study and corresponding transaxial slices are shown in Fig. 3. The [^{18}F]F-AraG image before MI shows a clear delineation of myocardium with noticeable uptake (Fig. 3C) but the [^{18}F]FDG uptake is blunted (Fig. 3D) indicating preferential use of free fatty acids (FFA) as energy substrates in the normal heart [27]. The [^{18}F]F-AraG uptake in the myocardium did not vary much after MI (Fig. 3C), while the [^{18}F]FDG signals showed wider variabilities at different time points (Fig. 3E, F) [28].

The distribution of [^{18}F]F-AraG and [^{18}F]FDG myocardial uptakes in terms of %ID/cc are shown in Fig. 4. There was a significant difference in %ID/cc between [^{18}F]F-AraG and [^{18}F]FDG signals in the normal myocardium (0.86 ± 0.12 vs. 0.32 ± 0.11, $p<0.001$) (Fig. 4A). The [^{18}F]FDG scans preformed before and after MI varied significantly between each time point (Fig. 4B). The variation of [^{18}F]FDG signals appears to be related to, in addition to the state and duration of fasting, diet, severity of infarction, the metabolic and hormonal state of each rat at the time of scanning. Although there were reduced activities in the infarct zones, the [^{18}F]F-AraG signals in the total myocardium did not show significant variation after MI from the baseline (0.86 ± 0.12 vs. 0.83 ± 0.08, $p=$ ns) (Fig. 4C).

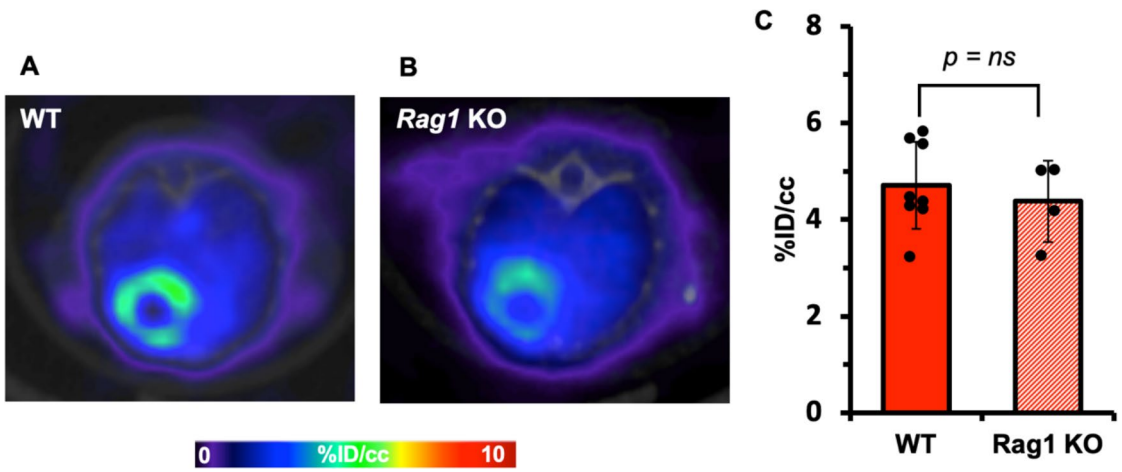

Fig. 2 Comparison of [^{18}F]F-AraG signals in the myocardium between WT (**A**) and *Rag1* KO (**B**) mice. The %ID/cc (**C**) for *Rag1* KO tend to be lower compared to WT mice but the difference is not statistically significant ($p=$ ns) indicating myocardial uptake is primarily coming from cardiomyocytes

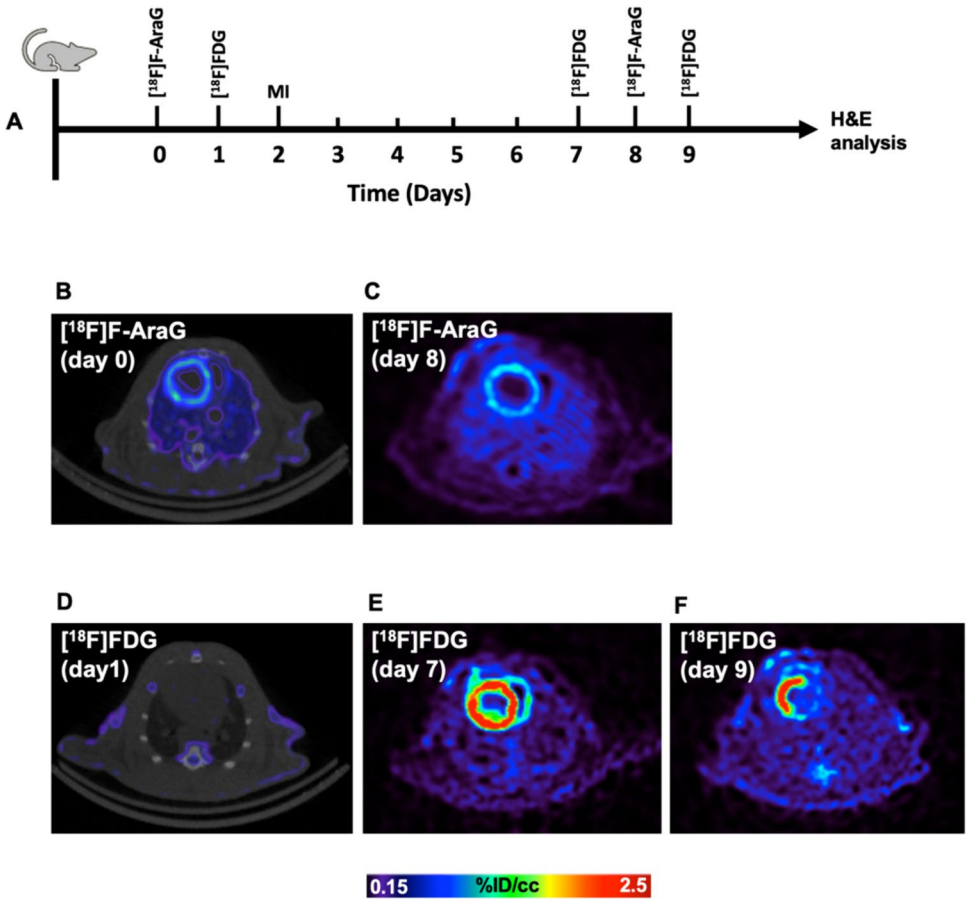

Fig. 3 (**A**) Rat study timeline. Comparison of [^{18}F]F-AraG signals in a rat before (**B**) and after (**C**) MI. There were no [^{18}F]FDG signals in the myocardium before MI (**D**) while the patterns of uptake differed on two different days after MI (**E**, **F**). All slices were from the midventricular section of the heart

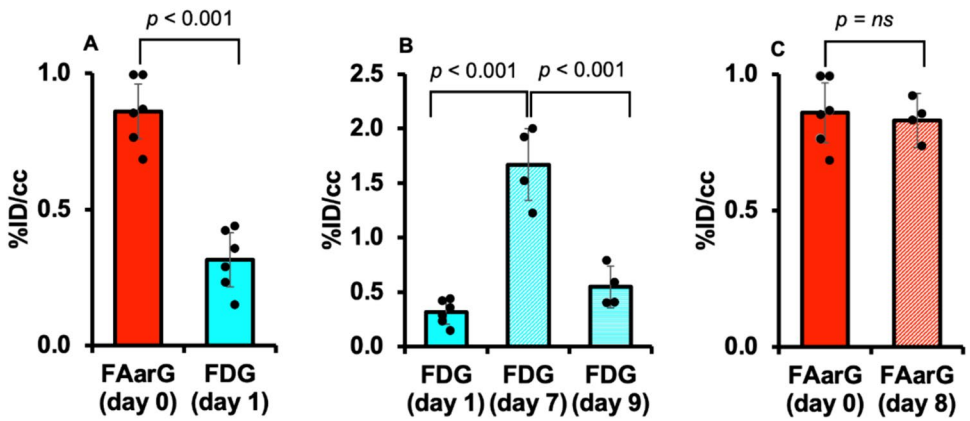

Fig. 4 (**A**) %ID/cc for [^{18}F]F-AraG and [^{18}F]FDG signals for 6 rats before MI. (**B**) [^{18}F]FDG signal variability in the myocardium at different time points after MI compared to baseline. There were significant differences in [^{18}F]FDG signals between different time points. (**C**) [^{18}F]F-AraG signals in the total myocardium tend to decrease after MI from the baseline but the difference was not statistically significant (p = ns)

Effects of Dietary Nucleotides on [^{18}F]F-AraG Myocardial Signal

Nucleotides are the building blocks of the nucleic acids and are necessary nutrients to maintain many different cellular functions including the mitochondrial energy metabolism [29]. To assess whether the myocardial [^{18}F]F-AraG uptake in normal heart varies on dietary nucleotides, we compared [^{18}F]F-AraG signals between mice fed with purified diet supplemented with nucleotides (PD + NT) with that without nucleotides (PD). No difference in myocardial uptake in terms of %ID/cc was observed between two groups indicating that the nucleotides do not have effect on [^{18}F]F-AraG myocardial uptake in normal heart (8.31 ± 0.88 vs. 7.72 ± 0.95, p = ns) (Fig. 5).

Assessing MI with [^{18}F]F-AraG and [^{18}F]FDG

The [^{18}F]FDG and [^{18}F]F-AraG signals are shown in Fig. 6A and B from middle ventricle to apical regions in a minimally

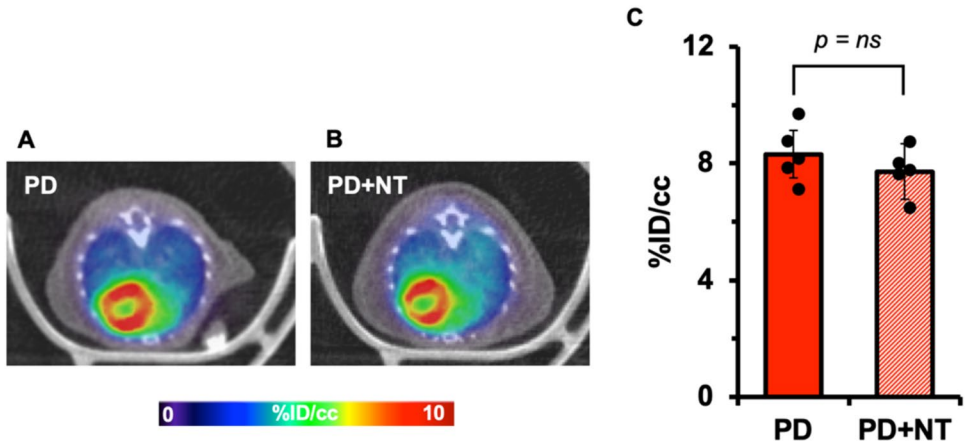

Fig. 5 Myocardial [^{18}F]F-AraG uptakes in mice fed with purified diet (PD) (**A**) and diet supplemented with nucleotides (PD + NT) (**B**). The difference in %ID/cc in two groups was not statistically significant (p = ns) indicating that [^{18}F]F-AraG uptake in myocardium does not vary with dietary nucleotides (**C**)

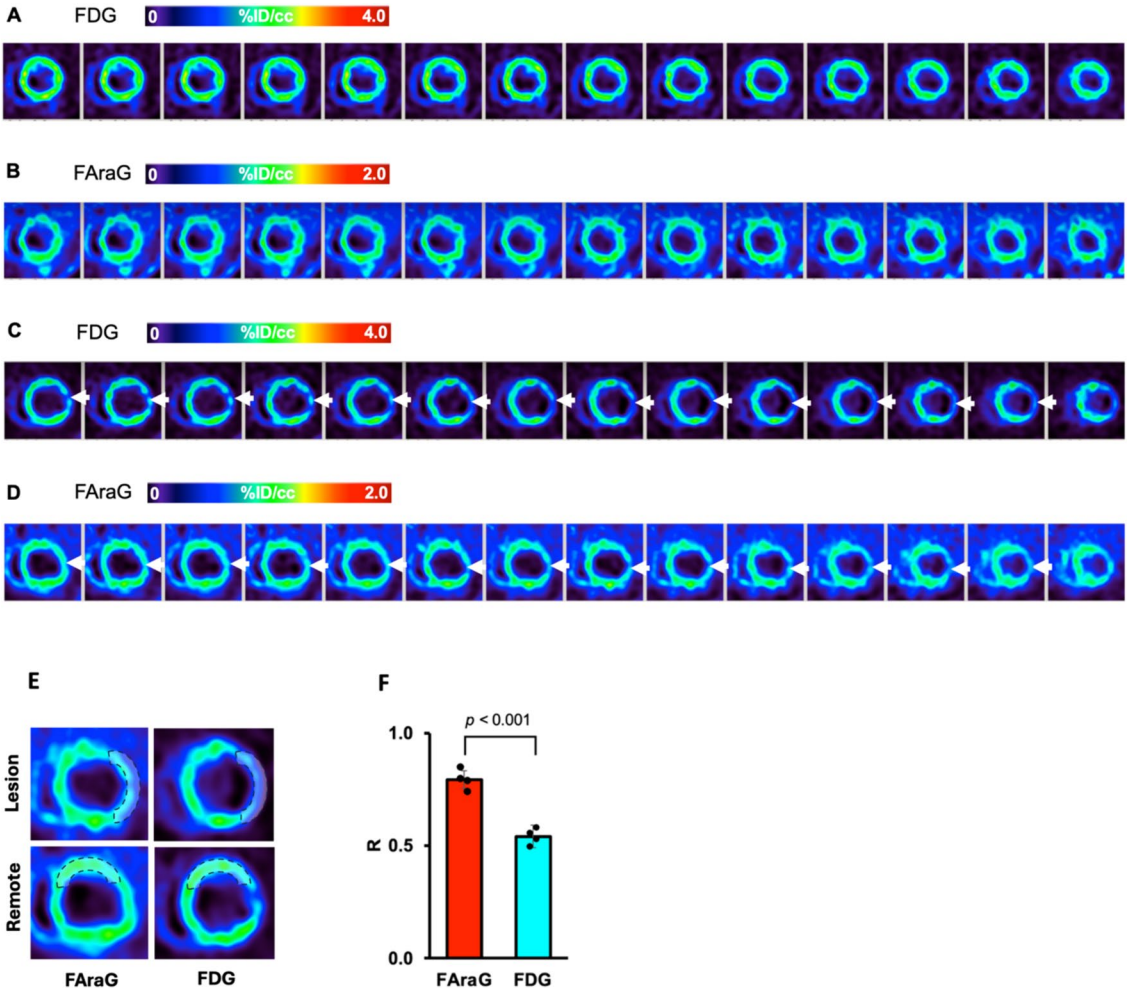

Fig. 6 Comparison of [^{18}F]FDG (**A**) and [^{18}F]F-AraG (**B**) signals in the myocardium of a least-affected rat heart after MI. Shown here are the mid ventricular slices in short-axis view. Comparison of [^{18}F]FDG (**C**) and [^{18}F]F-AraG (**D**) signals in the myocardium of another rat with significantly larger MI region. The extent of significantly reduced activity (indicated by arrows) in [^{18}F]FDG image extends from mid-ventricle down to apex in the inferior-lateral wall. A comparative study for the uptake ratios (R) between the MI region and remote region (**E**) indicates [^{18}F]F-AraG uptake ratio was significantly greater than that of [^{18}F]FDG (**F**)

affected rat heart following an MI. In this case, the boundary of the MI region was limited to near apex. Figure 5C and D display the myocardial slices of another rat with significantly larger MI region. The [^{18}F]FDG and [^{18}F]F-AraG images shown here are taken from day 7 and 8, respectively. There were significant reduced activities in the inferior-lateral wall in the mid ventricular region down to apex in the [^{18}F]FDG signal indicating MI to a broader extent. The arrows in the [^{18}F]FDG image slices show the regions with significantly reduced activity affected by the I/R injury that extends up to 5 mm longitudinally. Although the co-registered [^{18}F]F-AraG image slices showed a similar pattern of reduced intensity in the affected areas with significant wall thinning, there was a noticeable [^{18}F]F-AraG uptake in the MI regions indicating potential mitochondrial activity and thus presence of viable cardiomyocytes.

Although a significant thinning of myocardial wall was seen in the affected regions by both [^{18}F]FDG and [^{18}F]F-AraG, the regions of reduced tracer uptake were smaller in the [^{18}F]F-AraG image compared to that of [^{18}F]FDG image. The arrows in Fig. 6C and D highlight the disparities in uptake between [^{18}F]FDG and [^{18}F]F-AraG in the MI regions. We also examined uptake ratios (R) between the MI region and remote region for [^{18}F]FDG and [^{18}F]F-AraG by placing a volume within ROI (Fig. 6E). The [^{18}F]F-AraG uptake ratio was significantly higher than that of [^{18}F]FDG (0.79 ± 0.09 vs. 0.53 ± 0.06, $p < 0.001$), indicating potential mitochondrial activity in the MI region (Fig. 6F).

T Cell Infiltration Evaluated with IHC H&E Staining

To evaluate immune infiltration in the heart after injury we performed immunohistochemical staining of the hearts extracted one day post imaging. Figure 7 shows an example result from IHC H&E staining analysis for one of the rats. The decreased [^{18}F]FDG activity in Fig. 6 in the inferior-lateral wall, from the mid region down to the apex, corresponds to the mid-ventricular section in the H&E staining images, specifically aligning with the area exhibiting fibrosis (Top panels). While immunohistochemistry for CD3 indicates the presence of T cells, indicated with red arrow (Bottom right), in the fibrotic scarred area affected by myocardial infarction, T cells do not constitute the predominant infiltrates (Bottom panels). Out of 4 rats, only 2 showed myocardial fibrosis with the presence of T cells in H&E analysis.

Discussion

In this study we investigated the interplay between glucose metabolism and mitochondrial biogenesis in the heart after MI. The lower [^{18}F]FDG signal in the infarcted region indicates lower glucose metabolism in the injured cardiomyocytes and absence of rampant immune cell infiltration that might be accompanying the injury. The simultaneous reduction of glucose metabolism and mitochondrial activity in the infarct region as demonstrated by matched [^{18}F]FDG and [^{18}F]F-AraG images may indicate tissue fibrosis and scar buildup [30, 31]. However, presence of [^{18}F]F-AraG uptake in the region with substantially reduced [^{18}F]FDG uptake may indicate active mitochondrial biogenesis in viable cardiomyocytes.

One of the major functions of mitochondria is to produce energy via oxidative phosphorylation [29]. However, studies suggest that mitochondria not only produce energy, but they are also involved in many vital biological processes such as intracellular signaling, pyridine synthesis, phospholipid modifications and calcium regulation [32]. Mitochondrial dysfunction is considered a major orchestrator of cardiomyocyte death after MI. The homeostasis of any healthy cardiomyocyte implies a controlled regulation of mitochondrial activity via enhanced self-renewal (biogenesis) as an adaptive response to external stress such as hypoxia and is vital for the cell survivability [33]. The molecular mechanism

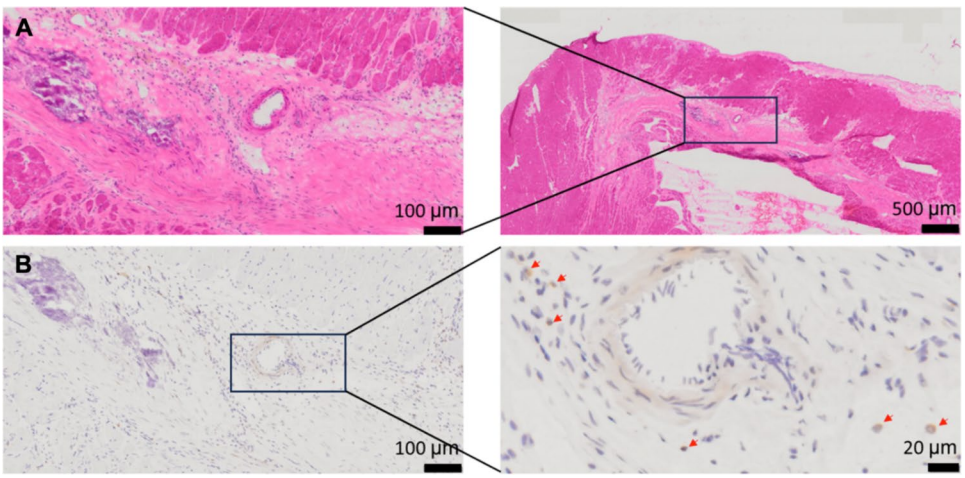

Fig. 7 Inflammatory infiltrates in myocardial infarction. The top panels display H&E stain results, highlighting myocardial inflammatory infiltrate and myocardial fibrosis (**A**). The bottom panels exhibit immunohistochemistry for CD3, showing the presence of T cells in the infarct area (**B**). CD3-positive T cells are specifically indicated with red arrows

behind the role of mitochondria on reducing damage to cardiomyocytes caused by oxidative stress are not fully understood [34]. However, noting the fact that glucose is the ultimate substrate in ischemia because of chronically reduced blood flow, the viable cardiomyocytes that do not take part in the contractility due to loss of metabolism might have persistent mitochondrial biogenesis reflected by the [^{18}F]F-AraG activity seen in the infarcted area (Fig. 6).

Ischemic heart disease has been shown to be associated with an excess production of reactive oxygen species (ROS) in the process of oxidation in mitochondria [35, 36]. In this process, the mitochondrial respiratory chain seems to be affected via ROS interference. Normal ROS production is necessary for healthy cellular signaling but its excess may have deleterious effect because it reacts with and damages mtDNA, decreases its copy number, and impairs mitochondrial gene transcription and protein expression via oxidation of large molecules [37]. Toxicity caused by ROS is likely to stimulate the transcription factor and nuclear gene expression required to activate mitochondrial biogenesis by oxidant-driven mechanism [38–40] that [^{18}F]F-AraG is deeply associated with.

Mitochondrial biogenesis is also required for activation and proliferation of T cells that may be infiltrating the injured heart. As [^{18}F]F-AraG accumulates in activated T cells, signal in the affected area may also be coming from infiltrating lymphocytes as a sign of chronic inflammation [41]. Histological analysis revealed myocardial fibrosis in the infarcted region and presence of T cells (Fig. 7). Considering the relatively low level of T cells infiltrates found in the affected regions, we expect [^{18}F]F-AraG accumulation in cardiomyocytes to be the predominant source of signal in the infarcted border zone. Imaging of T cell-deficient *Rag1* KO mice also showed that the [^{18}F]F-AraG signal in the normal heart is coming from cardiomyocytes and not from T cells (Fig. 2). Further study is needed to evaluate the [^{18}F]F-AraG signal differentiation between cardiomyocytes and T cell after MI.

In healthy subjects, heart gets most of its energy via oxidation of FFA. However, in ischemia, there is an upregulation of glucose transporters to switch towards glucose metabolism as a main substrate via nonmitochondrial pathway [42]. [^{18}F]FDG PET imaging has therefore been routinely used for testing myocardial viability noninvasively [43]. A major limitation of use of [^{18}F]FDG PET is its variability on blood glucose level, that depends on diet and duration of fasting, that necessitates a tedious, time-consuming protocol to achieve a diagnostic accuracy [44]. Particularly in diabetic patients, [^{18}F]FDG PET has been found to be less efficient due to frequent glucose monitoring and insulin administration. Moreover, the metabolic and hormonal state, which cannot be controlled experimentally, play a role on the [^{18}F]FDG variability and may give rise to different uptake values at different time points (Figs. 3, 4). Accumulation of [^{18}F]F-AraG in myocardium, by contrast, does not reflect glucose metabolism and may thus represent an [^{18}F]FDG PET alternative for viability assessment in diabetic as well as nondiabetic patients. Furthermore, it appears that [^{18}F]F-AraG uptake in the myocardium does not differ with the dietary nucleotides, at least in normal myocardium (Fig. 5). However, we do not know if there is variation in [^{18}F]F-AraG uptake with the dietary nucleotides in a diseased heart.

The minimal uptake of the [^{18}F]FDG in normal heart, as shown in Fig. 3, can be explained by the heart's energy metabolism. The normal heart selectively uses free fatty acids (FFA) as energy substrates, with most cellular ATP being derived from fatty acid oxidation [42]. High variability in MI is indeed interesting but expected based on the design of the experiment. Although we maintained overnight fasting for all animals, we did not monitor the exact fasting duration for each animal. While all animals were fed the same diet and followed the same anesthetic procedures, glucose levels were unknown because they were not measured. Hormone levels that can also be affecting [^{18}F]FDG uptake were not measured either.

There was higher background noise in the [^{18}F]F-AraG image compared to [^{18}F]FDG. But it may not be a potential concern since the overall average target-to-background ratio in the vicinity of heart is approximately 3:1 which indicates that the delineation of myocardium should not be affected by the background noise.

A comparative analysis of the ratio of the uptakes in the MI region to remote region (Fig. 6) showed [^{18}F]F-AraG ratio to be significantly higher than that of the [^{18}F]FDG indicative of potential mitochondrial activity in the MI region. However, we did not perform perfusion analysis to quantify the amount of viable tissue in the MI region to demonstrate the utility [^{18}F]F-AraG PET as a viability imaging agent.

Small sample size is a limitation of this study. Like for many other myocardial perfusion agents, [^{18}F]F-AraG's accumulation in the liver affected delineation of the MI region that might have affected the %ID/cc further signifying the importance of respiratory motion correction. Image resolution and partial volume effect are some of the factors that also degraded the image quality which might have affected the [^{18}F]FDG – [^{18}F]F-AraG image registration. The analysis was performed using predefined thresholds of $< 50\%$ cutoff for defining MI region without having auxiliary anatomical imaging such as MR. Other threshold could have resulted in slightly different results and should be included in any future study.

Conclusions

The PET imaging agent developed for activated T cells, [^{18}F]F-AraG, is suitable for cardiac imaging and has potential for assessing myocardial viability after MI. Further study with a larger sample size is needed to verify our preliminary results.

Acknowledgements This work was supported in part by gift from CellSight Technologies, Inc., and National Heart, Lung, and Blood Institute grant R01HL160688. Inveon microPET/CT (Siemens Medical Solutions) was purchased with the support of National Institutes of Health grant S10RR023051. NanoScan microPET/CT (Mediso USA), which replaced Inveon, was purchased with the grant supports of National Institutes of Health grant S10OD034286 and University of California, San Francisco.

Author Contributions UMS: Analyzed PET data, wrote manuscript,
HC: Coordinated animal study, conducted H&E analysis, wrote manuscript,
QF, RJL: Coordinated and participated in the ligation study, reviewed manuscript,
JP, LH: Participated in data acquisition, reviewed manuscript,
TLH: Coordinated microPET/CT animal imaging, reviewed manuscript,
HV, JB: Coordinated [^{18}F]F-AraG synthesis, reviewed manuscript,
JL, YS: Coordinated animal study, conceptualized the problem, reviewed data, edited manuscript.

Data Availability The data presented in this study are available upon appropriate request to corresponding authors.

Declarations

Conflicts of Interest JL and HC are employed by CellSight Technologies, Inc., which is developing [^{18}F]F-AraG for commercial use. JL holds patents related to [^{18}F]F-AraG.

References

1. Rezende PC et al (2019) Clinical significance of chronic myocardial ischemia in coronary artery disease patients. J Thorac Dis 11(3):1005–1015
2. Bender SR et al (2012) Electrocardiographic left ventricular hypertrophy predicts arrhythmia and mortality in patients with ischemic cardiomyopathy. J Interv Card Electrophysiol 34(3):237–245
3. Werner GS et al (2023) Three-year outcomes of a randomized multicentre trial comparing revascularization and optimal medical therapy for chronic total coronary occlusions (EuroCTO). EuroIntervention 19(7):571–579
4. Yager N, Schulman-Marcus J, Torosoff M (2021) Coronary anatomy and comorbidities impact on elective PCI outcomes in left main and multivessel coronary artery disease. Catheter Cardiovasc Interv 98(3):436–444
5. Bax JJ et al (2004) Extensive left ventricular remodeling does not allow viable myocardium to improve in left ventricular ejection fraction after revascularization and is associated with worse long-term prognosis. Circulation 110(11 Suppl 1):II18–22
6. Parodi O (1993) Non-invasive assessment of residual viability in post-myocardial infarction patients: role of nuclear techniques. Int J Card Imaging 9:19–29
7. Allman KC (2013) Noninvasive assessment myocardial viability: current status and future directions. J Nucl Cardiol 20(4):618–37; quiz 638–9
8. Demirkol MO (2008) Myocardial viability testing in patients with severe left ventricular dysfunction by SPECT and PET. Anadolu Kardiyol Derg 8(Suppl 2):60–70
9. Cahill TJ, Kharbanda RK (2018) Viability testing to guide myocardial revascularisation in patients with heart failure. Indian J Thorac Cardiovasc Surg 34(Suppl 3):206–212
10. Park JS et al (2023) Impact of positron emission tomography viability imaging: guided revascularizations on clinical outcomes in patients with myocardial scar on single-photon emission computed tomography scans. J Korean Med Sci 38(46):e399
11. Kazakauskaite E et al (2022) Comparative analysis of myocardial viability multimodality imaging in patients with previous myocardial infarction and symptomatic heart failure. Medicina (Kaunas) 58(3):368
12. Garcia MJ et al (2020) State of the art: imaging for myocardial viability: a scientific statement from the American Heart Association. Circ Cardiovasc Imaging 13(7):e000053
13. Levi J et al (2022) Biodistribution of a mitochondrial metabolic tracer, [(18)F]F-AraG, in healthy volunteers. Mol Imaging 2022:3667417
14. Ronald JA et al (2017) A PET imaging strategy to visualize activated t cells in acute graft-versus-host disease elicited by allogenic hematopoietic cell transplant. Cancer Res 77(11):2893–2902
15. Cohen MH et al (2008) FDA drug approval summary: nelarabine (Arranon) for the treatment of T-cell lymphoblastic leukemia/lymphoma. Oncologist 13(6):709–714
16. Leanza L et al (2010) Activation of guanine-beta-D-arabinofuranoside and deoxyguanosine to triphosphates by a common pathway blocks T lymphoblasts at different checkpoints. Exp Cell Res 316(20):3443–3453
17. Levi J et al (2019) Imaging of activated T cells as an early predictor of immune response to Anti-PD-1 therapy. Cancer Res 79(13):3455–3465
18. Levi J et al (2021) (18)F-AraG PET for CD8 Profiling of Tumors and Assessment of Immunomodulation by Chemotherapy. J Nucl Med 62(6):802–807
19. Franc BL et al (2017) *In Vivo* PET imaging of the activated immune environment in a small animal model of inflammatory arthritis. Mol Imaging 16:1536012117712638
20. Guglielmetti C et al (2022) Longitudinal imaging of T Cells and inflammatory demyelination in a preclinical model of multiple sclerosis using (18)F-FAraG PET and MRI. J Nucl Med 63(1):140–146
21. Omidvari N et al (2023) Total-body dynamic imaging and kinetic modeling of (18)F-AraG in healthy individuals and a non-small cell lung cancer patient undergoing anti-PD-1 immunotherapy. medRxiv. https://doi.org/10.1101/2023.09.22.23295860
22. Levi J, Song H (2022) The other immuno-PET: Metabolic tracers in evaluation of immune responses to immune checkpoint inhibitor therapy for solid tumors. Front Immunol 13:1113924
23. Peluso MJ et al (2024) Tissue-based T cell activation and viral RNA persist for up to 2 years after SARS-CoV-2 infection. Sci Transl Med 16(754):eadk3295
24. Namavari M et al (2011) Synthesis of 2'-deoxy-2'-[18F]fluoro-9-beta-D-arabinofuranosylguanine: a novel agent for imaging T-cell activation with PET. Mol Imaging Biol 13(5):812–818
25. Klocke R et al (2007) Surgical animal models of heart failure related to coronary heart disease. Cardiovasc Res 74(1):29–38
26. Loening AM, Gambhir SS (2003) AMIDE: a free software tool for multimodality medical image analysis. Mol Imaging 2(3):131–137

27. Stanley WC, Recchia FA, Lopaschuk GD (2005) Myocardial substrate metabolism in the normal and failing heart. Physiol Rev 85(3):1093–1129
28. Haider A et al (2020) Myocardial (18)F-FDG uptake pattern for cardiovascular risk stratification in patients undergoing oncologic PET/CT. J Clin Med 9(7)
29. Spinelli JB, Haigis MC (2018) The multifaceted contributions of mitochondria to cellular metabolism. Nat Cell Biol 20(7):745–754
30. Khalaf S, Al-Mallah MH (2020) Fluorodeoxyglucose applications in cardiac PET: viability, inflammation, infection, and beyond. Methodist Debakey Cardiovasc J 16(2):122–129
31. Bengel FM et al (2009) Cardiac positron emission tomography. J Am Coll Cardiol 54(1):1–15
32. Wang L (2016) Mitochondrial purine and pyrimidine metabolism and beyond. Nucleosides Nucleotides Nucleic Acids 35(10–12):578–594
33. Zhou H et al (2021) Role of mitochondrial quality surveillance in myocardial infarction: From bench to bedside. Ageing Res Rev 66:101250
34. Dai DF, Rabinovitch PS (2009) Cardiac aging in mice and humans: the role of mitochondrial oxidative stress. Trends Cardiovasc Med 19(7):213–220
35. Kibel A et al (2020) Oxidative stress in ischemic heart disease. Oxid Med Cell Longev 2020:6627144
36. Dhalla NS et al (1999) Evidence for the role of oxidative stress in acute ischemic heart disease: a brief review. Can J Cardiol 15(5):587–593
37. Bliksoen M et al (2015) Mitochondrial DNA damage and repair during ischemia-reperfusion injury of the heart. J Mol Cell Cardiol 78:9–22
38. Geldon S, Fernandez-Vizarra E, Tokatlidis K (2021) Redox-mediated regulation of mitochondrial biogenesis, dynamics, and respiratory chain assembly in yeast and human cells. Front Cell Dev Biol 9:720656
39. Piantadosi CA, Suliman HB (2012) Redox regulation of mitochondrial biogenesis. Free Radic Biol Med 53(11):2043–2053
40. Suliman HB et al (2004) Lipopolysaccharide induces oxidative cardiac mitochondrial damage and biogenesis. Cardiovasc Res 64(2):279–288
41. Nevers T et al (2015) Left Ventricular T-Cell Recruitment Contributes to the Pathogenesis of Heart Failure. Circ Heart Fail 8(4):776–787
42. Lopaschuk GD, Stanley WC (1997) Glucose metabolism in the ischemic heart. Circulation 95(2):313–315
43. Al Moudi M, Sun ZH (2014) Diagnostic value of (18)F-FDG PET in the assessment of myocardial viability in coronary artery disease: a comparative study with (99m)Tc SPECT and echocardiography. J Geriatr Cardiol 11(3):229–36
44. Dilsizian V (2016) Highlights from the Updated Joint ASNC/SNMMI PET Myocardial Perfusion and Metabolism Clinical Imaging Guidelines. J Nucl Med 57(9):1327–1328